Published in final edited form as:

Neuroscience. 2015 April 16; 291: 155–166. doi:10.1016/j.neuroscience.2015.01.069.

BMP signaling and microtubule organization regulate synaptic strength

Robin W. Ball[1], **Einat Peled**[1], **Giovanna Guerrero**[1,3], and **Ehud Y. Isacoff**[1,2,#]

[1]Department of Molecular and Cell Biology and the Helen Wills Neuroscience Institute, University of California, Berkeley, CA 94720

[2]Physical Bioscience Division, Lawrence Berkeley National Laboratory, Berkeley, CA 94720

Abstract

The strength of synaptic transmission between a neuron and multiple postsynaptic partners can vary considerably. We have studied synaptic heterogeneity using the glutamatergic *Drosophila* neuromuscular junction (NMJ), which contains multiple synaptic connections of varying strength between a motor axon and muscle fiber. In larval NMJs, there is a gradient of synaptic transmission from weak proximal to strong distal boutons. We imaged synaptic transmission with the postsynaptically targeted fluorescent calcium sensor SynapCam, to investigate the molecular pathways that determine synaptic strength and set up this gradient. We discovered that mutations in the Bone Morphogenetic Protein (BMP) signaling pathway disrupt production of strong distal boutons. We find that strong connections contain unbundled microtubules in the boutons, suggesting a role for microtubule organization in transmission strength. The *spastin* mutation, which disorganizes microtubules, disrupted the transmission gradient, supporting this interpretation. We propose that the BMP pathway, shown previously to function in the homeostatic regulation of synaptic growth, also boosts synaptic transmission in a spatially selective manner that depends on the microtubule system.

Keywords

Drosophila; neuromuscular junction; synaptic transmission; Bone Morphogenetic Protein signalling pathway; microtubule; fluorescent calcium sensor

[#]To whom correspondence should be addressed: ehud@berkeley.edu, (510) 642-9853.
[3]Present address: Ciencia Puerto Rico, Rio Piedras, PR 00927

Author contributions: RWB, GG and EYI designed experiments; RWB and EP performed experiments; RWB analyzed the data; RWB and EYI wrote the paper.

The authors declare no conflict of interest.

Introduction

A neuron in the mammalian brain typically makes multiple connections with its postsynaptic partners. These synapses can differ significantly in transmission strength. The heterogeneity may result from differences in the assemblies of pre- and postsynaptic proteins, in the history of activity-dependent plasticity, or in the homeostatic processes that adjust input to output and balance excitation and inhibition (Dobrunz and Stevens, 1997, Murthy et al., 1997, Koester and Sakmann, 2000, Turrigiano and Nelson, 2004, Froemke et al., 2005, Dean and Dresbach, 2006, Pozo and Goda, 2010, Sun et al., 2013). These complex phenomena can be studied in the synapses of simpler model systems, which possess many of the mammalian molecular components and also show synaptic plasticity and homeostasis, such as the glutamatergic *Drosophila* larval NMJ. During the larval stages, the body wall muscles grow ~100-fold and there is a corresponding increase in the length of the innervating motor axon, the number of boutons, the number of active zones, and the overall quantal content, which together ensure sufficient synaptic excitation to drive contraction (Schuster et al., 1996).

Members of the conserved BMP signaling pathway are important for this structural and physiological strengthening of the NMJ (Aberle et al., 2002, Marques et al., 2002, Haghighi et al., 2003, McCabe et al., 2003, Rawson et al., 2003, McCabe et al., 2004). The BMP ligand Glass Bottom Boat is thought to be released from the muscle and to act retrogradely on the axon by triggering a signaling cascade that involves the BMP Type II receptor Wishful Thinking (Wit), the Type I BMP receptors Saxophone and Thick Veins, and the Smad and co-Smad transcriptional regulators which they activate (Aberle et al., 2002, Marques et al., 2002, McCabe et al., 2003, Rawson et al., 2003, McCabe et al., 2004). One of the target genes of the Smads has been identified recently as *trio*, a regulator of the actin cytoskeleton (Ball et al., 2010). Although there appears to be a connection with the actin cytoskeleton, the molecular mechanism by which the BMP pathway controls synaptic function at the NMJ is for the most part unknown. Investigations of this retrograde pathway are relevant for understanding neural development in other systems, because recent studies have shown that the BMP pathway also controls the development of synapses in the mammalian brain (Kalinovsky et al., 2011, Xiao et al., 2013).

Axonal growth and transmission strength may also be regulated by the microtubule cytoskeleton and its associated proteins, which form the tracks along which synaptic vesicles, proteins and organelles are transported to the ends of the axon (Guzik and Goldstein, 2004). In fact, it has been reported that axonal transport is disrupted in BMP mutants (Aberle et al., 2002, Wang et al., 2007). To examine the roles of the BMP pathway and microtubules in the regulation of synaptic strength, we used SynapCam, a synaptically-targeted fluorescent Ca^{2+} sensor, with which it is possible to image glutamatergic transmission in the NMJ (Guerrero et al., 2005). We previously discovered a gradient of synaptic transmission strength at muscle 6 and now find that this pattern is disrupted in BMP pathway mutants. We find that the strongest boutons in wildtype larvae (at axon ends) and in BMP mutants (randomized spatially) often have unbundled microtubules, suggesting a role for microtubule organization in the regulation of synaptic transmission. In agreement with this, the gradient is also disrupted in larvae with genetically altered microtubule

organization. The results suggest that retrograde BMP signaling could affect synaptic homeostasis through regulation of microtubules.

Experimental Procedures

Fly Lines

SynapCam3.1 (SC3.1) flies in the *w1118* background were used for all functional imaging experiments (Guerrero et al., 2005). SynapCam was crossed into mutant backgrounds to create the following flies: *SC3.1;;wit^{HA3}/TM6B, SC3.1;;wit^{HA2}/TM6B, SC3.1;OK6-Gal4/Cyo^{GFP}; wit^{A12}/TM6B, SC3.1;UAS-Wit2A/Cyo^{GFP};wit^{B11}/TM6B* (*wit* flies from Corey Goodman Lab), *SC3.1;Mad^{1}/Cyo^{YFP}, SC3.1, BG380-Gal4; Mad^{k00237}/Cyo^{GFP} (abbreviated Mad^{237}), SC3.1;Df(2L)Exel^{7015}/Cyo^{YFP}* (*Mad* mutants from Brian McCabe and Pejmun Haghighi), *SC3.1,futsch^{N94}, SC3.1,futsch^{K68}* (from Graeme Davis), *SC3.1;;fmr$^{\Delta 50}$/TM6B, SC3.1;;fmr$^{\Delta 113}$/TM6B* (from Kendal Broadie), *SC3.1;;spastin$^{5.75}$/TM6B* (*spastin* mutant from Kai Zinn) and *SC3.1;OK6-Gal4/Cyo^{GFP}, SC3.1;;24B-Gal4, SC3.1;;UAS-Spas-RNAi* (Spastin RNAi flies from Andrea Daga). For quantification of Wit-GFP we used *Elav-Gal4/+;;UAS-Wit-GFP/+* and *OK6-Gal4/+;UAS-Wit-GFP/+* (UAS-Wit-GFP from Guillermo Marques). For quantification of mitochondria we used *D42-Gal4, UAS-mito-GFP/TM6* (from Bloomington Stock Center).

Electrophysiology and Optical Recording

We followed similar procedures and used the same equipment as previously described (Guerrero et al., 2005). Briefly, type Ib boutons in female 3rd instar larvae were used for all experiments. Muscle 6 from segments A2 or A3 were two electrode voltage clamped at −100 mV (for wildtype, *wit* at 1.5 mM Ca^{2+}, *Mad/+;wit/+*, *fmr*, *futsch* and *spastin* mutants) or −120 mV (for *wit* and *Mad* at 2 mM Ca^{2+}). All recordings were done at room temperature in physiological HL3 solution (Stewart et al., 1994) with 20 mM Mg^{+2}, plus 2–4 μM thapsigargin and 500 μM ryanodine to prevent muscle contraction. We found that ryanodine had no major effect on contraction and stopped using it for most of the data collected (neither thapsigargin nor ryanodine had a major impact on physiology or imaging results). The amount of Ca^{2+} in the solution was either 1.5 or 2 mM, as stated in the results section, but was always the same for direct comparisons between two genotypes (Table 1).

Larvae were imaged with either an ORCA-ER (Hamamatsu, Bridgewater, NJ) or Andor IQ (Andor, Belfast, Ireland) CCD camera (the camera had no effect on the patterns of synaptic transmission). All imaging experiments were done on an Olympus BX-50WI microscope (Olympus, Melville NY) with a 60×/0.9 water objective, and with an excitation filter of 434 ± 10 nm and a 460 nm dichroic filter. CFP and YFP emissions were separated with a dual-emission beam splitter (Optical Insights, Santa Fe NM) with a 510 nm dichroic filter and 480 ± 20 nm and 535 ± 20 nm emission filters. ΔFRET was defined as YFP/CFP emission of one image before nerve stimulation subtracted from another image directly after stimulation. The ΔFRET was averaged for 30–100 trials for each NMJ and reported as the raw value (not percentage) with arbitrary units. For all transmission gradient experiments “n” refers to the number of neuromuscular junctions recorded from each genotype. Only axon branches with 4 or more boutons (up to 12) were used to assess the presence of the

gradient. In order to facilitate direct comparisons, examples of ΔFRET images for mutants were chosen that had similarly shaped NMJs as the wildtype examples.

Immunohistochemistry

Immediately after optical recordings, flies were fixed for 10–20 mins in 4% formaldehyde. We used 1:100 mouse anti-Futsch (22c10, Developmental Studies Hybridoma Bank (DSHB), Univ of Iowa), 1:10,000 rabbit anti-VGlut (Daniels et al., 2004) (gift of Aaron DiAntonio), 1:50 mouse anti-Syntaxin (8C3, DSHB), 1:500 anti-Tubulin (T6074, Sigma), 1:500 rabbit anti-Phospho-Smad3 (EP823Y, AbCam), goat anti-HRP-Cy3 (1:100, Jackson ImmunoResearch Laboratories, West Grove, PA), goat anti-mouse and anti-rabbit Alexa647 (1:1000, Molecular Probes, Eugene, OR) and goat anti-GFP Alexa488 (1:500, Molecular Probes). Antibody stains were imaged on a Zeiss 510 Axioplan confocal or Zeiss 780 AxioExaminer confocal (Oberkochen, Germany) with a 63×/1.4 oil objective. Scale bars = 5 μm throughout paper.

Data Analysis

All SynapCam imaging data were initially analyzed using *Matlab 7.0* (Mathworks, Natick MA) as previously reported (Guerrero et al., 2005). When quantifying the correlation between strength and Futsch organization (as in Fig. 4C), the ΔFRETs were normalized to the strongest postsynapse in each NMJ and then averaged for boutons that had loops or diffuse staining (unbundled Futsch) and those that had bundled Futsch. The average ΔFRETs were compared using Student's two-tailed t-test to determine statistical significance in *Excel* (Microsoft, Redmond, WA). Significance was indicated on graphs by asterisks, where * $p < 0.05$, ** $p < 0.01$, *** $p < 0.005$. To quantify the transmission gradient, the ΔFRETs were plotted against postsynapse position for each NMJ and fit with a linear function. The slopes for each NMJ within a genotype were then averaged. All means are reported with standard error.

Results

Synaptic transmission decreased in *wit* mutants

To measure synaptic strength at multiple boutons with single bouton resolution, we expressed SynapCam, a ratiometric fluorescent Ca^{2+} sensor based on Cameleon 3.1 (Miyawaki et al., 1999), in the *Drosophila* larval muscle. SynapCam is localized near postsynaptic densities and responds to Ca^{2+} permeating glutamate receptors with a change in fluorescence resonance energy transfer (ΔFRET) (Guerrero et al., 2005). SynapCam imaging has previously revealed a gradient in synaptic transmission strength between the motor neuron and muscle 6 of wildtype 3rd instar larvae, with distal boutons being the strongest and proximal the weakest (Guerrero et al., 2005) (Fig. 1). The transmission gradient has been confirmed with chemical Ca^{2+} dyes in the motor axon innervating muscle 6 (Lnenicka et al., 2006, Muller and Davis, 2012). Although the purpose of the gradient on a single muscle remains unknown, the transmission gradient at muscle 6 offers us a convenient means with which we can monitor changes of synaptic activity and understand the cellular mechanisms that regulate transmission strength.

To investigate the patterns of synaptic strength further we imaged SynapCam in a null mutant of the presynaptic type II BMP receptor *wishful thinking (wit)*. *wit* mutants have reduced axon length and numbers of boutons and a decrease in excitatory junctional potential amplitude and quantal content, which is an estimate of the amount of vesicle release (Wan et al., 2000, Aberle et al., 2002, Marques et al., 2002, McCabe et al., 2004). Although *wit* mutants have smaller NMJs, there are still axon branches with multiple boutons in a row, so we focused on these longer branches for our experiments. SynapCam expressed well in wit^{HA2}/wit^{HA3} mutants, but the ΔFRET signal from SynapCam was barely detectable at the physiological concentration of external Ca^{2+} (1.5 mM) (Fig. 1). Thus, synaptic transmission at each bouton is impaired, which is consistent with electron micrographs showing abnormal ultrastructure of the active zones in *wit* mutants (Aberle et al., 2002).

Transmission gradient disrupted in *wit* mutants

Because of the reduced synaptic transmission, we imaged the BMP mutants at elevated Ca^{2+} concentration (2 mM) so that the ΔFRET levels would be large enough to visualize with accuracy. The increase in Ca^{2+} boosts the SynapCam signal in two ways: it augments transmitter release and it increases the driving force for Ca^{2+} entry through the glutamate receptors. We also used a more negative holding potential (−120 mV) to further increase the driving force for Ca^{2+} entry via the glutamate receptors. Wildtype NMJs were also recorded at 2 mM Ca^{2+}, to obtain the same conditions at the presynaptic side, but were held at −100 mV to avoid muscle contraction, which occurred at −120 mV (see Table 1 for recording conditions for each experiment). The holding potential should have no effect on the transmission gradient since it will affect the driving force across all postsynapses equally within each NMJ.

SynapCam imaging at 2 mM Ca^{2+} revealed that *wit* lacked the polarized transmission gradient seen in wildtype animals (Fig. 2A–F). The average ΔFRET for each position along a branch clearly showed that wildtype retains the synaptic gradient at elevated Ca^{2+}, but that the gradient is disrupted in *wit* mutants (Fig. 2D–E). If the average slope of a line fit to the data in Fig. 2D–E is negative, this would indicate that there is a gradient, with distal postsynapses having the strongest response. Indeed, wildtype had a negative slope (−0.0038 ± 0.0007) and *wit* had a positive slope that was close to zero (0.0011 ± 0.0013). These slopes were significantly different from each other ($p = 0.0017$). The gradients were further analyzed by comparing the ΔFRETs for the distal and most proximal postsynapses (Fig 2F). Since the NMJs were all different lengths, the most proximal postsynapse was at different distances from the end in different NMJs. In wildtype the average ΔFRET was 0.0502 ± 0.0044 for the distal position and 0.0275 ± 0.0035 for the most proximal position, which was significantly different ($p < 0.0001$). In contrast, in the wit^{HA2}/wit^{HA3} mutant there was no significant difference between the ΔFRETs in the distal position (0.0198 ± 0.0026) compared to the proximal position (0.0185 ± 0.0031, $p = 0.55$), further demonstrating that the transmission gradient is disrupted by the *wit* mutation.

To confirm that the disruption of the synaptic gradient in the *wit* mutant is specifically caused by mutation of that gene, we did a presynaptic rescue of the *wit* mutant. We found

that the gradient was completely restored when we expressed Wit only presynaptically using OK6-Gal4 in the wit^{A12}/wit^{B11} mutant background (Fig. 2C, F). There was a significant difference between the ΔFRETs in the distal (0.0622 ± 0.0115) and proximal positions (0.0267 ± 0.0068, p=0.0078). The rescue confirms that Wit acts presynaptically and that the transmission gradient is a property of the motor neurons, as previously reported (Guerrero et al., 2005).

The transmission gradient depends on Mad signaling

Wit can act through the canonical BMP signaling pathway, but it has also been shown to interact locally with LIM Kinase1 to maintain synapse stability (Eaton and Davis, 2005). To test if the effects of the transmission gradient are mediated through the rest of the BMP pathway, we focused on *Mad* mutants. Mad (Mothers Against Dpp) is the *Drosophila* Smad transcription factor and mutations in the gene cause similar defects in growth and transmission as *wit* (McCabe et al., 2004). We first recorded from double heterozygous mutants for *Mad* and *wit*. These NMJs still had a transmission gradient as evidenced by the significantly different ΔFRETs for proximal and distal postsynapses (Fig 3D, p = 0.0019), which is not surprising given the minimal effect of this mutant combination on NMJ growth (McCabe et al., 2004). We next recorded from two different *Mad* mutant alleles over a deficiency. As we observed in the *wit* mutant, the *Mad* mutants had lowered transmission strength and needed to be imaged at 2 mM Ca^{2+} with a muscle holding potential of −120 mV in order to obtain large enough SynapCam signals for the analysis.

The transmission gradient was altered by the *Mad* mutants in such a way that proximal and distal postsynapses were equally strong (Fig. 3A–D). The slope of the relation between ΔFRET and postsynapse position for the $Mad^{1}/Df(2L)Exel^{7015}$ mutant was close to zero (−0.00093 ± 0.00043), significantly different from wildtype (p = 0.0005), but not different from *wit* (p = 0.11). The average normalized ΔFRETs for distal postsynapses compared to proximal postsynapses in two different *Mad* mutants were not significantly different ($Mad^{1}/Df(2L)Exel^{7015}$ p = 0.077, $Mad^{237}/Df(2L)Exel^{7015}$ p = 0.11) (Fig 3D). In the *Mad* mutants, the weakest postsynapses were actually the middle ones (Fig. 3C). Like wildtype, the first few postsynapses after the distal position were significantly weaker than the distal postsynapse (position 1 vs. 2: p = 0.00026, 1 vs. 3: p = 0.0011). In wildtype, the transmission strength remains weak throughout the length of the axon to the proximal position, but in *Mad* mutants, the more proximal postsynapses increase in ΔFRET back to a level similar to the distal postsynapse (Fig. 3C–D). This is noticeably different from *wit* where the ΔFRET values are more randomly distributed throughout the axon (Fig. 2E). Although the gradient is clearly disrupted in both mutants, this difference between them may be due to the fact that the Wit receptor can also initiate cellular signals independent of Mad and transcription regulation (Eaton and Davis, 2005).

In summary, mutations in the BMP pathway both decrease transmission and rearrange the normal pattern of synaptic transmission strength. The results show that these mutations flatten the transmission gradient by reducing the strength of distal boutons to levels similar to weak proximal boutons in physiological Ca^{2+} concentration. This indicates that the overall reduction in quantal content in these mutants is due to a decrease of synaptic strength

at normally strong distal boutons. Thus, the canonical BMP signaling pathway appears to play a role in boosting synaptic strength selectively at distal boutons.

Since the BMP pathway acts to increase synaptic strength at distal boutons, we wondered if there is a correlation between synaptic strength and Wit receptor levels at the NMJ. We thought there might be higher levels of Wit receptors localized at distal boutons, which could activate BMP signaling more at the ends of axons. Endogenous Wit is undetectable with the available antibody (Aberle et al., 2002), so we overexpressed a UAS-Wit-GFP transgene presynaptically using the pan-neuronal driver Elav-Gal4 or the motor neuron driver OK6-Gal4 (Marques et al., 2003, Smith et al., 2012). We found that Wit-GFP expression was constant along the length of the axon (Fig. 3E–F), suggesting that the synaptic gradient is not due to differences in Wit distribution along the length of the axon.

Strong postsynapses are correlated with unbundled microtubules

While BMP signaling may lead the axon to establish stronger boutons at the ends of branches, what molecular mechanism could generate the gradient? We wondered if microtubules might be important for synaptic strength, because they provide the tracks along which synaptic machinery is transported to the presynaptic endings. A reason for suspecting that this might be the case is that strong boutons were typically observed at the ends of axonal branches and occasionally at axonal kinks, locations where it seemed likely that microtubule organization differed from elsewhere (Guerrero et al., 2005). It is difficult to get a clear image of microtubules at the NMJ, because they are located both in the boutons and in the muscle. In order to visualize presynaptic microtubules alone, SynapCam-imaged preparations were stained for Futsch, the *Drosophila* homolog of the mammalian Microtubule Associated Protein 1B, which co-localizes with microtubule bundles that run down the length of the axon (Roos et al., 2000). These bundles have been shown to unbundle in certain locations and either form loops or develop a diffuse organization, predominantly at terminal boutons, and occasionally at other locations along the motor neuron axon (Roos et al., 2000, Ruiz-Canada et al., 2004). Following SynapCam imaging of wildtype larvae, the larvae were stained for Futsch to reveal the location of unbundled microtubules. In wildtype larvae, unbundled microtubules were often found at strong end boutons, as well as at the few proximal boutons that showed strong transmission (Fig. 4A–D). This association between unbundling of microtubules and stronger transmission was also seen in *wit* and *Mad* mutants. Even though the transmission at these mutant boutons is weaker than in wildtype, they vary in strength (Fig. 2 and 3) and we found the strongest *wit* and *Mad* boutons to typically contain unbundled Futsch (Fig. 4C and data not shown). This was true regardless of the location of the strong boutons in the axon or the concentration of Futsch in the loop (Fig. 4D). In contrast, weak boutons correlated with bundled Futsch both in wildtype and *wit* NMJs (Fig. 4C). Despite the association of unbundled microtubules with strong transmission, transmission strength is clearly not completely dependent on microtubule structure, since unbundled microtubules could also be found in weak boutons and bundled microtubules could be found in strong boutons (Fig. 4E–H). Nevertheless, the correlation suggests that microtubule organization may be one of the determinants of a bouton’s transmission strength.

The synaptic gradient does not require Futsch

Having seen that microtubule structure is correlated with synaptic strength, we next asked whether disruption of proteins that regulate microtubule architecture would also disrupt the transmission gradient. We first turned to Futsch itself, which is particularly interesting because it is a downstream effector of the BMP pathway at the NMJ and helps stabilize microtubules (Ellis et al., 2010, Nahm et al., 2013). We performed SynapCam recordings in two *futsch* mutants, both of which have been reported to have disordered microtubule structure in the axon and reduced number of boutons (Roos et al., 2000). In some larvae of these *futsch* mutants we confirmed that tubulin staining sometimes filled up the entire bouton and there was increased microtubule looping (Fig. 5C). However, in other *futsch* larvae with the same genotype, the microtubules still formed bundles down the length of the axon, as seen in wildtype larvae (Fig. 5A–B). Therefore, the disordered microtubule phenotype is not of uniform severity in the *futsch* mutants.

In addition, we recorded from a mutant of the *fmr* gene, which codes for the Fragile X Mental Retardation Protein and represses Futsch protein expression (Zhang et al., 2001), enabling us to assess the impact of Futsch overexpression. We found the *futsch* mutants and the *fmr* mutant to have distal-proximal transmission gradients, similar to wildtype NMJs (Fig. 4I–L). As in wildtype (Fig. 2F), the ΔFRET was significantly larger at distal postsynapses than at proximal postsynapses for all three genotypes ($futsch^{N94}$: distal 0.0313 ± 0.0036, proximal 0.0144 ± 0.0020, $p < 0.0001$; $futsch^{K68}$: distal 0.0405 ± 0.0051, proximal 0.0153 ± 0.0023, $p < 0.001$; *fmr*: distal 0.0525 ± 0.0052, proximal 0.0296 ± 0.0040, $p < 0.0001$). Both *futsch* and *fmr* mutants have altered NMJ structures, so it is interesting to note that changes to NMJ growth can occur without disruption of the synaptic gradient. These results suggest that Futsch is not involved in regulating the spatial distribution of synaptic strength.

Transmission gradient disrupted in mutant with altered microtubule organization

Having found an association between synaptic strength and microtubule organization, but no connection with Futsch levels, we next set out to test this relationship through another genetic perturbation of microtubules. We turned to null mutation of *spastin*, a mutant with drastically altered microtubule organization. Spastin encodes an AAA ATPase that cleaves microtubules (Sherwood et al., 2004). The *spastin* mutant has a different effect on motor axon development from the mutations that decrease or increase Futsch levels, resulting in greater number of boutons, increased axon branching, fewer Futsch and microtubule loops and decreased tubulin in terminal boutons (Fig. 5E, 6A–D) (Sherwood et al., 2004, Orso et al., 2005). SynapCam imaging revealed that at physiological Ca^{2+} (1.5 mM) transmission strength in *spastin* is slightly weaker than wildtype along the entire length of the axon. When external Ca^{2+} was elevated to 2 mM, SynapCam imaging revealed that the transmission gradient is disrupted in *spastin* (Fig. 6E–F). The slope of the relation between ΔFRET and postsynapse position was close to zero (−0.00036 ± 0.00061) and was significantly different from the wildtype slope ($p = 0.001$), but not from *wit* ($p = 0.39$). There was no significant difference between the ΔFRET measured at distal and proximal postsynapses (Fig. 6I) (distal = 0.0285 ± 0.0032, proximal = 0.0231 ± 0.0035, $p = 0.096$).

Spastin is expressed both presynaptically in motor neurons and postsynaptically in body wall muscles (Sherwood et al., 2004), so we wanted to test if the effect on the transmission gradient of the *spastin* mutation is due to a presynaptic effect that could be attributed to the microtubules in the axon. We used a UAS-Spastin-RNAi line that was shown previously to alter microtubule structure, but in a different way than the null mutation: levels of acetylated-Tubulin and microtubule loops are both increased (Trotta et al., 2004). We recorded from NMJs in which Spastin-RNAi was expressed exclusively presynaptically under control of the OK6-Gal4 driver or postsynaptically with the 24B-Gal4 driver. SynapCam imaging was performed at 1.5 mM Ca^{2+} for both the Spastin-RNAi and the OK6-Gal4 control because synaptic transmission was not reduced by Spastin-RNAi (Fig. 6G–I). As in wildtype NMJs, the OK6-Gal4 control showed a synaptic gradient, with a significant difference between ΔFRETs for distal postsynapses (0.0393 ± 0.0044) and proximal postsynapses (0.0273 ± 0.0042, p = 0.0032). Likewise, when Spastin-RNAi was expressed in muscles, the synaptic gradient was not altered (distal = 0.0321 ± 0.018, proximal = 0.0162 ± 0.0064, p = 0.0072). In contrast, presynaptic expression of the Spastin RNAi disrupted the synaptic transmission gradient (Fig. 6H–I) so that there was no significant difference between the ΔFRETs for distal and proximal postsynapses (distal = 0.0316 ± 0.0062, proximal = 0.0269 ± 0.0058, p = 0.152).

We wondered if the importance of presynaptic Spastin for the generation of the transmission gradient might arise from an effect on the BMP signaling pathway, such that the *spastin* mutant might decrease BMP activity. To assess this, we stained motor neuron cell bodies and nuclei for phosphorylated Mad (P-Mad), which is decreased in mutants of the BMP ligand or receptors (Marques et al., 2003, McCabe et al., 2003). We found that not only was P-Mad staining not decreased in the *spastin* mutant, as one would expect if BMP signaling were decreased, it was actually increased (Fig. 6J), suggesting that Spastin may play a role in internalization of Wit, as has been shown for the related protein Spartin (Nahm et al., 2013). The results from the *spastin* mutant and *spastin* RNAi support the hypothesis that microtubule organization plays a role in establishing the proximo-distal transmission gradient along axon branches.

Discussion

As the *Drosophila* larval body wall muscles grow during development, the retrograde BMP signaling pathway helps regulate the concomitant increase in both the number of innervating boutons and transmitter release, which together maintain synaptic homeostasis (Schuster et al., 1996, Aberle et al., 2002, Marques et al., 2002, Haghighi et al., 2003, McCabe et al., 2003, Rawson et al., 2003, McCabe et al., 2004). Mutations in the BMP pathway reduce both axon growth and quantal content. Because of the strong effects of BMP pathway mutants on growth, it has been difficult to directly determine if they functionally impair synaptic transmission or if the effect is a by-product of perturbed growth. There are examples at the *Drosophila* NMJ of specific forms of synaptic homeostasis that do not affect synaptic growth, but depend upon intact BMP signaling (Haghighi et al., 2003, Goold and Davis, 2007).

To further study the role of the BMP signaling pathway in regulating synaptic transmission, we used SynapCam, a synaptically-targeted fluorescent Ca^{2+} sensor (Guerrero et al., 2005), to image glutamatergic transmission at the developing *Drosophila* larval NMJ. This method enables visualization of transmission with single bouton resolution. We asked how the distribution of transmission strength is affected by mutations in the BMP pathway.

BMP pathway mutations weaken synaptic transmission and disrupt the spatial gradient

We found that mutations in the presynaptic type II receptor, Wit, and the Smad transcription factor, Mad, led to weakened total postsynaptic SynapCam signals, consistent with the electrophysiologically measured reduction in quantal content. Indeed, transmission in the mutants is comparable to what is seen at the weakest proximal boutons in wildtype animals. The transmission that remains in *wit* and *Mad* is not homogeneous, but among these weak boutons the relative strength is not distributed in an orderly gradient. Thus, the selective strengthening of distal boutons is absent when BMP signaling is disrupted. Our observations indicate that BMP signaling boosts the strength of synaptic transmission, which organizes the proximo-distal gradient of transmission strength at muscle 6.

Microtubule organization affects distribution of synaptic strength

Having tied BMP signaling to the selective strengthening of synaptic transmission at distal boutons we searched for the cellular mechanism by which this is accomplished. A clue came from a report that at the *Drosophila* NMJ, presynaptic α-tubulin and acetylated-tubulin levels are decreased in *thick veins* mutants (one of the BMP Type I receptors) and that axonal transport is disrupted in a number of BMP mutants, including *wit* (Wang et al., 2007). In addition, the BMP pathway was recently shown to increase microtubule stability via regulation of Futsch by Fragile X Mental Retardation Protein (Nahm et al., 2013). We examined microtubule structure by looking at Futsch staining and observed that strong boutons often contain a specialized microtubule architecture: unbundled microtubules, seen as either microtubule loops or diffusely distributed microtubules. The correlation between unbundled microtubules and strong transmission suggests that unbundled microtubules support the delivery, or modification, of molecules, which boost synaptic transmission.

To probe the role of microtubules in the patterning of synaptic strength, we examined the effect of mutants that alter the level of Futsch, which has a role in organizing microtubules. Futsch mutation has a mild effect on axon growth, and Futsch levels are decreased in BMP mutants (Roos et al., 2000, Ellis et al., 2010). We found no effect of raising or lowering Futsch levels on the transmission gradient. This suggests that the disruption of the transmission gradient by BMP pathway mutants is not mediated through Futsch. In contrast, mutation or presynaptic RNAi suppression of the AAA+ ATPase Spastin, a protein which severs microtubules (Sherwood et al., 2004), had a dramatic effect on axon morphology, disrupted both the localization of unbundled microtubules to terminal boutons and disrupted the transmission gradient. Interestingly, it has been shown that the *spastin* mutant has decreased levels of acetylated-tubulin, similar to what is seen in the type 1 BMP receptor mutant, *thick veins* (Yao et al., 2011).

There are a number of other proteins that are also associated with microtubules, which may play a role in setting up the pattern of synaptic strength. For instance, overexpression of the microtubule associated protein Tau in motor neurons, which disrupts axonal transport and decreases the number of presynaptic mitochondria, causes major defects in synaptic growth and synaptic transmission (Chee et al., 2005). Interestingly, other mutations that interfere with mitochondrial delivery to nerve terminals decrease the number of microtubule loops and impair transmission (Guo et al., 2005). In hippocampal neurons, mobile mitochondria transported on microtubules influence the variability of synaptic strength (Sun et al., 2013). However, we did not detect a concentration gradient of mitochondria in the motor axon (Fig. 7), so mitochondria themselves cannot be the determinant of the transmission gradient.

Super resolution imaging has recently shown that end boutons in the *Drosophila* NMJ have larger active zones and more Bruchpilot (Brp) within each active zone (Ehmann et al., 2014). Brp clusters Ca^{2+} channels and vesicles at the active zone, so this could presumably affect the strength of synaptic transmission. Interestingly, in pyramidal and dentate gyrus neurons, there is also a transmission gradient, where the presynaptic terminals closest to the soma are strongest (de Jong et al., 2012). The strength of these synapses correlates with presynaptic components such as VGlut, synaptotagmin and syntaxin. In contrast, we did not see concentration gradients of the vesicular glutamate transporter (VGlut), suggesting a uniform distribution of synaptic vesicles, or Syntaxin (Syx), a member of the vesicle docking apparatus (Fig. 7). Rab3, which is an active zone GTPase, has also been shown to have an even distribution at the NMJ, though mutation of *rab3* does disrupt the transmission gradient (Peled and Isacoff, 2011). While the proteins that set up the transmission gradient have yet to be identified, and the mechanism underlying their inhomogeneous distribution remains to be defined, our suggestion that microtubules are involved is supported by the recent findings by others of inhomogeneous distribution of overexpressed dynactin, which is involved in retrograde axonal transport, and dense core vesicles during anterograde transport (Lloyd et al., 2012, Wong et al., 2012).

Conclusion

Our experiments reveal a new role for the BMP signaling pathway in the motor axon of the *Drosophila* larval NMJ. We find that the BMP signaling pathway, which was earlier implicated in structural homeostasis (McCabe et al., 2003) and physiological homeostasis (Haghighi et al., 2003), acts to set the global level of transmission strength and organizes the spatial distribution of synaptic strength in the presynaptic axon. This is accomplished by a selective boost in the strength of particular boutons, which, in muscle 6, are the distal boutons. How does such polarized regulation occur? We find that the spatial organization of transmission strength correlates to microtubule structure in the presynaptic axon. Given the recent findings that the BMP pathway is necessary for microtubule-based axonal transport and microtubule stability, we propose that BMP signaling controls synaptic transmission strength via the regulation of microtubules. In line with this model, changes in synaptic strength during presynaptic long-term potentiation in the hippocampus are dependent on microtubule-based axonal transport (Barnes et al., 2010).

It is not clear how BMP signaling produces the proximo-distal spatial organization of microtubule architecture and transmission strength. Release of the only known Wit ligand at the NMJ, Glass Bottom Boat, has not yet been directly observed and so its spatial distribution of signaling is unknown. However, one can imagine that different strengths of BMP signaling could selectively strengthen certain inputs and could underlie the wide range in transmission properties between active zones at the NMJ (Peled and Isacoff, 2011).

Acknowledgements

We thank Camellia Asgarian, Grant Kauwe and Gautam Agarwal for technical assistance, and Kristin Scott and members of the Isacoff Lab for advice and comments on the manuscript. We thank Brian McCabe, Pejmun Haghighi, Kai Zinn, Andrea Daga, Graeme Davis, Kendal Broadie and Guillermo Marques for fly lines, and Aaron DiAntonio and the Developmental Studies Hybridoma Bank at the University of Iowa for antibodies. This work was supported by a National Institutes of Health graduate fellowship (R.W.B.), HHMI predoctoral fellowship (G.G.), National Institutes of Health grant R01NS050833 and National Science Foundation grant FIBR 0623527.

References

Aberle H, Haghighi AP, Fetter RD, McCabe BD, Magalhaes TR, Goodman CS. wishful thinking encodes a BMP Type II Receptor that regulates synaptic growth in Drosophila. Neuron. 2002; 33:545–558. [PubMed: 11856529]

Ball RW, Warren-Paquin M, Tsurudome K, Liao EH, Elazzouzi F, Cavanagh C, An BS, Wang TT, White JH, Haghighi AP. Retrograde BMP signaling controls synaptic growth at the NMJ by regulating trio expression in motor neurons. Neuron. 2010; 66:536–549. [PubMed: 20510858]

Barnes SJ, Opitz T, Merkens M, Kelly T, von der Brelie C, Krueppel R, Beck H. Stable mossy fiber long-term potentiation requires calcium influx at the granule cell soma, protein synthesis, and microtubule-dependent axonal transport. J Neurosci. 2010; 30:12996–13004. [PubMed: 20881117]

Chee FC, Mudher A, Cuttle MF, Newman TA, MacKay D, Lovestone S, Shepherd D. Over-expression of tau results in defective synaptic transmission in Drosophila neuromuscular junctions. Neurobiol Dis. 2005; 20:918–928. [PubMed: 16023860]

Daniels RW, Collins CA, Gelfand MV, Dant J, Brooks ES, Krantz DE, DiAntonio A. Increased expression of the Drosophila vesicular glutamate transporter leads to excess glutamate release and a compensatory decrease in quantal content. J Neurosci. 2004; 24:10466–10474. [PubMed: 15548661]

de Jong AP, Schmitz SK, Toonen RF, Verhage M. Dendritic position is a major determinant of presynaptic strength. J Cell Biol. 2012; 197:327–337. [PubMed: 22492722]

Dean C, Dresbach T. Neuroligins and neurexins: linking cell adhesion, synapse formation and cognitive function. Trends Neuro. 2006; 29:21–29.

Dobrunz LE, Stevens CF. Heterogeneity of release probability, facilitation, and depletion at central synapses. Neuron. 1997; 18:995–1008. [PubMed: 9208866]

Eaton BA, Davis GW. LIM Kinase1 controls synaptic stability downstream of the type II BMP receptor. Neuron. 2005; 47:695–708. [PubMed: 16129399]

Ehmann N, van de Linde S, Alon A, Ljaschenko D, Keung XZ, Holm T, Rings A, DiAntonio A, Hallermann S, Ashery U, Heckmann M, Sauer M, Kittel RJ. Quantitative super-resolution imaging of Bruchpilot distinguishes active zone states. Nature communications. 2014; 5:4650.

Ellis JE, Parker L, Cho J, Arora K. Activin signaling functions upstream of Gbb to regulate synaptic growth at the Drosophila neuromuscular junction. Dev Biol. 2010; 342:121–133. [PubMed: 20346940]

Froemke RC, Poo MM, Y D. Spike-timing-dependent synaptic plasticity depends on dendritic location. Nature. 2005; 434:221–225. [PubMed: 15759002]

Goold CP, Davis GW. The BMP ligand Gbb gates the expression of synaptic homeostasis independent of synaptic growth control. Neuron. 2007; 56:109–123. [PubMed: 17920019]

Guerrero G, Reiff DF, Agarwal G, Ball RW, A B, CS G, EY I. Heterogeneity in synaptic transmission along a Drosophila larval motor axon. Nature Neuroscience. 2005; 8:1188–1196.

Guo X, Macleod GT, Wellington A, Hu F, Panchumarthi S, Schoenfield M, Marin L, Charlton MP, Atwood HL, Zinsmaier KE. The GTPase dMiro is required for axonal transport of mitochondria to Drosophila synapses. Neuron. 2005; 47:379–393. [PubMed: 16055062]

Guzik BW, Goldstein LSB. Microtubule-dependent transport in neurons: steps towards an understanding of regulation, function and dysfunction. Curr Opin Cell Bio. 2004; 16:443–450. [PubMed: 15261678]

Haghighi AP, McCabe BD, Fetter RD, Palmer JE, Hom S, Goodman CS. Retrograde control of synaptic transmission by postsynaptic CaMKII at the Drosophila neuromuscular junction. Neuron. 2003; 39:255–267. [PubMed: 12873383]

Kalinovsky A, Boukhtouche F, Blazeski R, Bornmann C, Suzuki N, Mason CA, Scheiffele P. Development of axon-target specificity of ponto-cerebellar afferents. PLoS Biol. 2011; 9:e1001013. [PubMed: 21346800]

Koester HJ, Sakmann B. Calcium dynamics associated with action potentials in single nerve terminals of pyramidal cells in layer 2/3 of the young rat neocortex. J Physiol. 2000; 529(Pt 3):625–646. [PubMed: 11118494]

Lloyd TE, Machamer J, O'Hara K, Kim JH, Collins SE, Wong MY, Sahin B, Imlach W, Yang Y, Levitan ES, McCabe BD, Kolodkin AL. The p150(Glued) CAP-Gly domain regulates initiation of retrograde transport at synaptic termini. Neuron. 2012; 74:344–360. [PubMed: 22542187]

Lnenicka GA, Grizzaffi J, Lee B, Rumpal N. Ca2+ dynamics along identified synaptic terminals in Drosophila larvae. J Neurosci. 2006; 26:12283–12293. [PubMed: 17122054]

Marques G, Bao H, Haerry TE, Shimell MJ, Duchek P, Zhang B, O'Connor MB. The Drosophila BMP type II receptor Wishful Thinking regulates neuromuscular synapse morphology and function. Neuron. 2002; 33:529–543. [PubMed: 11856528]

Marques G, Haerry TE, Crotty ML, Xue M, Zhang B, O'Connor MB. Retrograde Gbb signaling through the Bmp type 2 receptor wishful thinking regulates systemic FMRFa expression in Drosophila. Development. 2003; 130:5457–5470. [PubMed: 14507784]

McCabe BD, Hom S, Aberle H, Fetter RD, Marques G, Haerry TE, Wan H, O'Connor MB, Goodman CS, Haghighi AP. Highwire regulates presynaptic BMP signaling essential for synaptic growth. Neuron. 2004; 41:891–905. [PubMed: 15046722]

McCabe BD, Marqués G, Haghighi AP, Fetter RD, Crotty ML, Haerry TE, Goodman CS, O'Conner MB. The BMP homolog Gbb provides a retrograde signal that regulates synaptic growth at the Drosophila neuromuscular junction. Neuron. 2003; 39:241–254. [PubMed: 12873382]

Miyawaki A, Griesbeck O, Heim R, Tsien R. Dynamic and quantitative Ca21 measurements using improved cameleons. PNAS. 1999; 96:2135–2140. [PubMed: 10051607]

Muller M, Davis GW. Transsynaptic control of presynaptic ca(2+) influx achieves homeostatic potentiation of neurotransmitter release. Curr Biol. 2012; 22:1102–1108. [PubMed: 22633807]

Murthy VN, Sejnowski TG, Stevens CF. Heterogeneous release properties of visualized individual hippocampal synapses. Neuron. 1997; 18:599–612. [PubMed: 9136769]

Nahm M, Lee MJ, Parkinson W, Lee M, Kim H, Kim YJ, Kim S, Cho YS, Min BM, Bae YC, Broadie K, Lee S. Spartin Regulates Synaptic Growth and Neuronal Survival by Inhibiting BMP-Mediated Microtubule Stabilization. Neuron. 2013; 77:680–695. [PubMed: 23439121]

Orso G, Martinuzzi A, Rossetto MG, Sartori E, Feany M, Daga A. Disease-related phenotypes in a Drosophila model of hereditary spastic paraplegia are ameliorated by treatment with vinblastine. J Clin Invest. 2005; 115:3026–3034. [PubMed: 16276413]

Peled ES, Isacoff EY. Optical quantal analysis of synaptic transmission in wild-type and rab3-mutant Drosophila motor axons. Nat Neurosci. 2011; 14:519–526. [PubMed: 21378971]

Pozo K, Goda Y. Unraveling mechanisms of homeostatic synaptic plasticity. Neuron. 2010; 66:337–351. [PubMed: 20471348]

Rawson JM, Lee M, Kennedy EL, Selleck SB. Drosophila neuromuscular synapse assembly and function require the TGF-beta type I receptor saxophone and the transcription factor Mad. J Neurobiol. 2003; 55:134–150. [PubMed: 12672013]

Roos J, Hummel T, Ng N, Klambt C, Davis GW. Drosophila Futsch regulates synaptic microtubule organization and is necessary for synaptic growth. Neuron. 2000; 26:371–382. [PubMed: 10839356]

Ruiz-Canada C, Ashley J, Moeckel-Cole S, Drier E, Yin J, Budnik V. New synaptic bouton formation is disrupted by misregulation of microtubule stability in aPKC mutants. Neuron. 2004; 42:567–580. [PubMed: 15157419]

Schuster CM, Davis GW, Fetter RD, Goodman CS. Genetic dissection of structural and functional components of synaptic plasticity. I. Fasciclin II controls synaptic stabilization and growth. Neuron. 1996; 17:641–654. [PubMed: 8893022]

Sherwood NT, Sun Q, Xue M, Zhang B, Zinn K. Drosophila Spastin regulates synaptic microtubule networks and is required for normal motor function. PLoS Biol. 2004; 2:2094–2111.

Smith RB, Machamer JB, Kim NC, Hays TS, Marques G. Relay of retrograde synaptogenic signals through axonal transport of BMP receptors. J Cell Sci. 2012; 125:3752–3764. [PubMed: 22573823]

Stewart BA, Atwood HL, Renger JJ, Wang J, Wu CF. Improved stability of Drosophila larval neuromuscular preparations in haemolymph-like physiological solutions. J Comp Physiol [A]. 1994; 175:179–191.

Sun T, Qiao H, Pan PY, Chen Y, Sheng ZH. Motile axonal mitochondria contribute to the variability of presynaptic strength. Cell Rep. 2013; 4:413–419. [PubMed: 23891000]

Trotta N, Orso G, Rossetto MG, Daga A, Broadie K. The hereditary spastic paraplegia gene, spastin, regulates microtubule stability to modulate synaptic structure and function. Curr Biol. 2004; 14:1135–1147. [PubMed: 15242610]

Turrigiano GG, Nelson SB. Homeostatic plasticity in the developing nervous system. Nature rev neuro. 2004; 5:97–107.

Wan HI, DiAntonio A, Fetter RD, Bergstrom K, Strauss R, Goodman CS. Highwire regulates synaptic growth in Drosophila. Neuron. 2000; 26:313–329. [PubMed: 10839352]

Wang X, Shaw WR, Tsang HT, Reid E, O'Kane CJ. Drosophila spichthyin inhibits BMP signaling and regulates synaptic growth and axonal microtubules. Nat Neurosci. 2007; 10:177–185. [PubMed: 17220882]

Wong MY, Zhou C, Shakiryanova D, Lloyd TE, Deitcher DL, Levitan ES. Neuropeptide delivery to synapses by long-range vesicle circulation and sporadic capture. Cell. 2012; 148:1029–1038. [PubMed: 22385966]

Xiao L, Michalski N, Kronander E, Gjoni E, Genoud C, Knott G, Schneggenburger R. BMP signaling specifies the development of a large and fast CNS synapse. Nat Neurosci. 2013; 16:856–864. [PubMed: 23708139]

Yao A, Jin S, Li X, Liu Z, Ma X, Tang J, Zhang YQ. Drosophila FMRP regulates microtubule network formation and axonal transport of mitochondria. Hum Mol Genet. 2011; 20:51–63. [PubMed: 20935173]

Zhang YQ, Bailey AM, Matthies HJ, Renden RB, Smith MA, Speese SD, Rubin GM, Broadie K. Drosophila fragile X-related gene regulates the MAP1B homolog Futsch to control synaptic structure and function. Cell. 2001; 107:591–603. [PubMed: 11733059]

Highlights

- Synaptic transmission strength was imaged using a postsynaptic calcium indicator
- The proximal-distal gradient of synaptic strength is disrupted in BMP mutants
- Unbundled MAP1B, found in loops, is associated with stronger boutons
- Alterations in microtubule structure impair the synaptic transmission gradient

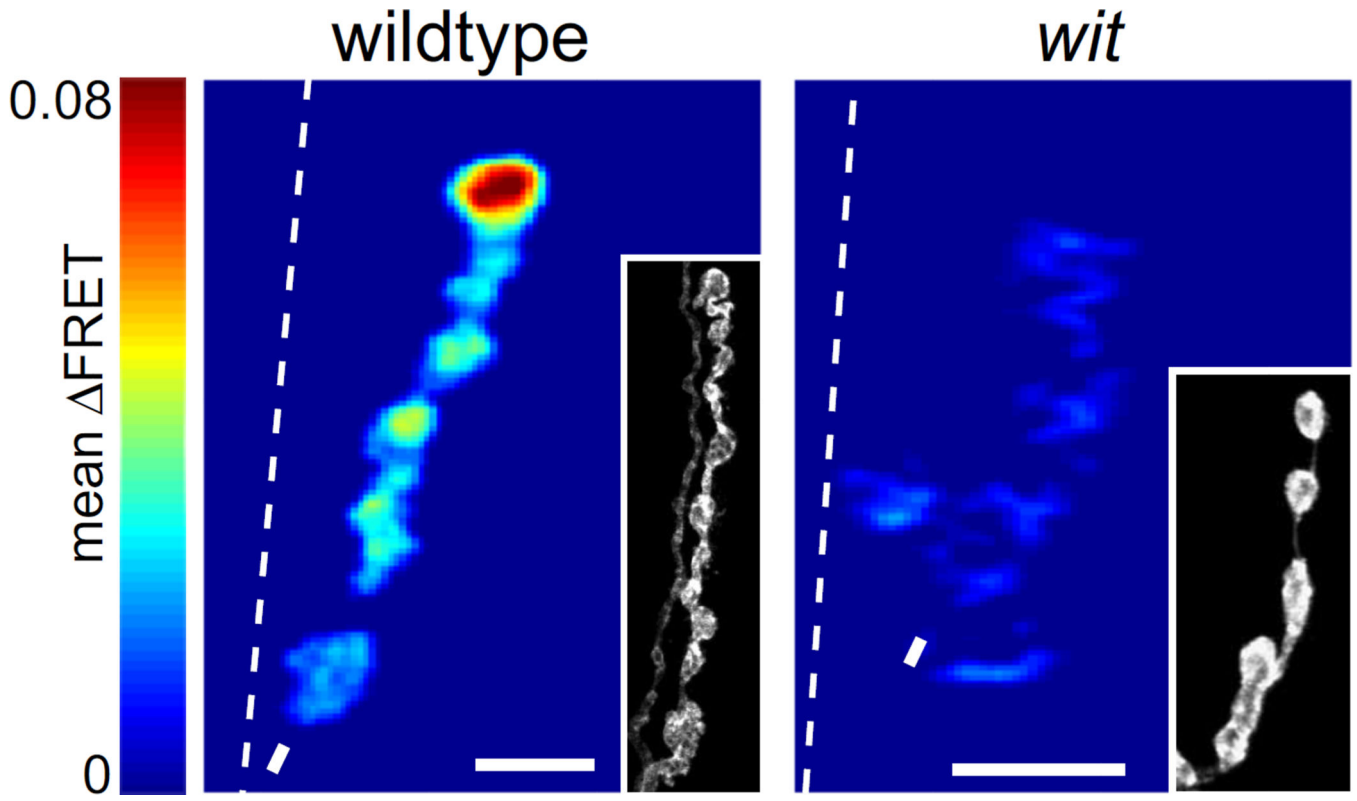

Figure 1.

Synaptic transmission is decreased in *wit* mutants. Mean SynapCam ΔFRET for wildtype and wit^{HA2}/wit^{HA3} at 1.5 mM Ca^{2+} all on the same pseudocolor scale for ΔFRET (scale: 0–0.08). Throughout the paper, asterisks mark distal ends, dashed lines are borders between muscle 6 and 7, and arrows are where axons enter muscle or branchpoints. Insets: HRP stain showing the morphology of the NMJ. Scale bars = 5 μm throughout paper.

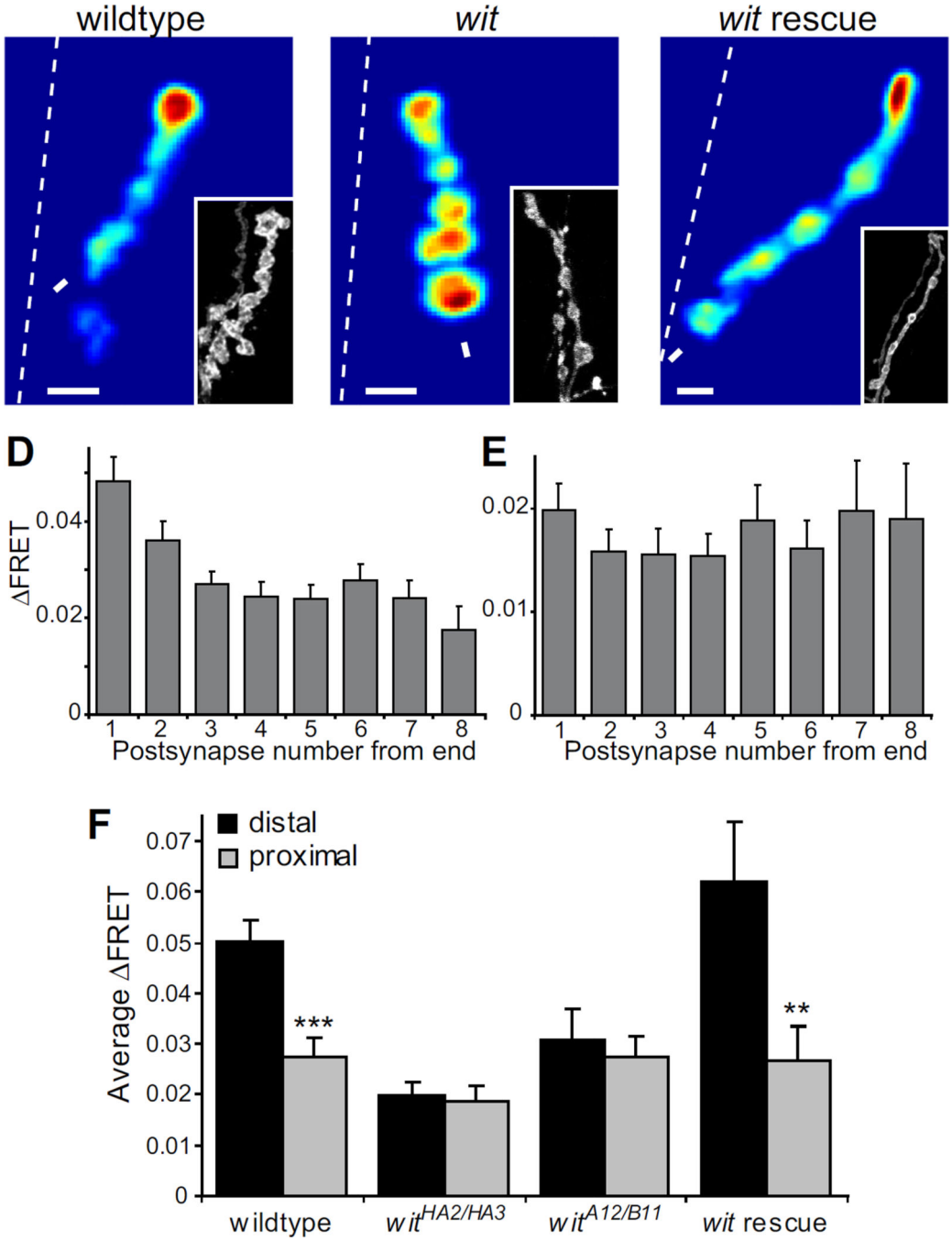

Figure 2.

The transmission gradient is disrupted in *wit* mutants. (A–C) Mean ΔFRET of (A) wildtype (scale:0–0.13), (B) $wit^{HA2/HA3}$ (scale:0–0.055), and (C) Wit presynaptic rescue (*SynapCam;OK6-Gal4/UAS-Wit2A;* wit^{A12}/wit^{B11}, scale:0–0.17) recorded in 2 mM Ca^{2+}. (D, E) Average ΔFRET versus postsynaptic location (with the distal end being #1) for (D) wildtype (n = 21 NMJs) and (E) $wit^{HA2/HA3}$ (n = 21). (F) Average ΔFRET of distal postsynapse versus proximal postsynapse. There is a significant difference (student's paired t-test) between distal and proximal ΔFRET in wildtype and the presynaptic Wit rescue, but

not in either *wit* mutant ($wit^{HA2/HA3}$ and *UAS-Wit2A/+;* wit^{A12}/wit^{B11}, *n = 11*). Error bars are SEM throughout paper.

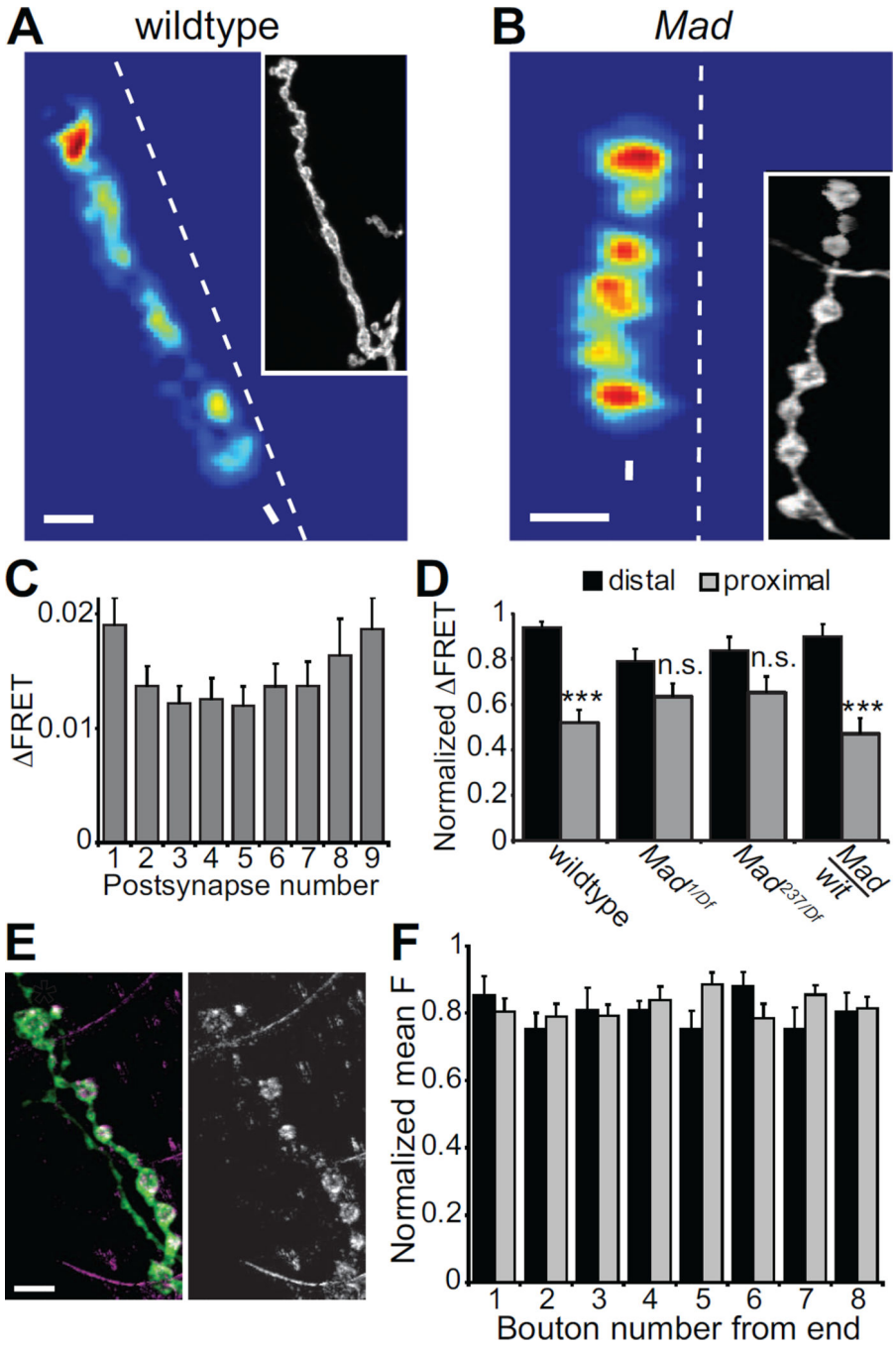

Figure 3.

Transmission gradient requires Mad. (A–B) Mean ΔFRET of (A) wildtype (scale:0–0.06) and (B) *Mad*^{1}*/Df(2L)Exel*^{7015} mutant (scale:0–0.03) at 2 mM Ca^{2+}. (C) Average of all *Mad*^{1}*/Df(2L)Exel*^{7015} ΔFRETs versus location in the branch (n = 28). (D) Average ΔFRET of the most distal and proximal postsynapses in each branch normalized to the strongest postsynapse in each NMJ. The ΔFRETs are not significantly different (n.s.) in *Mad*^{1}*/Df(2L)Exel*^{7015} (n = 28) and *Mad*^{237}*/Df(2L)Exel*^{7015} (n = 16) mutants, but they are different in *Mad*^{237}*/+;wit*^{A12}*/+* (n = 10). (E) An NMJ expressing Wit-GFP presynaptically (*Elav-*

Gal4/+;;UAS-Wit-GFP/+). Left image shows HRP stain in green and Wit-GFP in purple. The same Wit-GFP staining is shown alone on right in white. The asterisk indicates the distal bouton. (F) The normalized mean fluorescence from Wit-GFP expressed with Elav-Gal4 (black bars) or OK6-Gal4 (grey bars) for each bouton in a string, with bouton #1 being the most distal (n = 10).

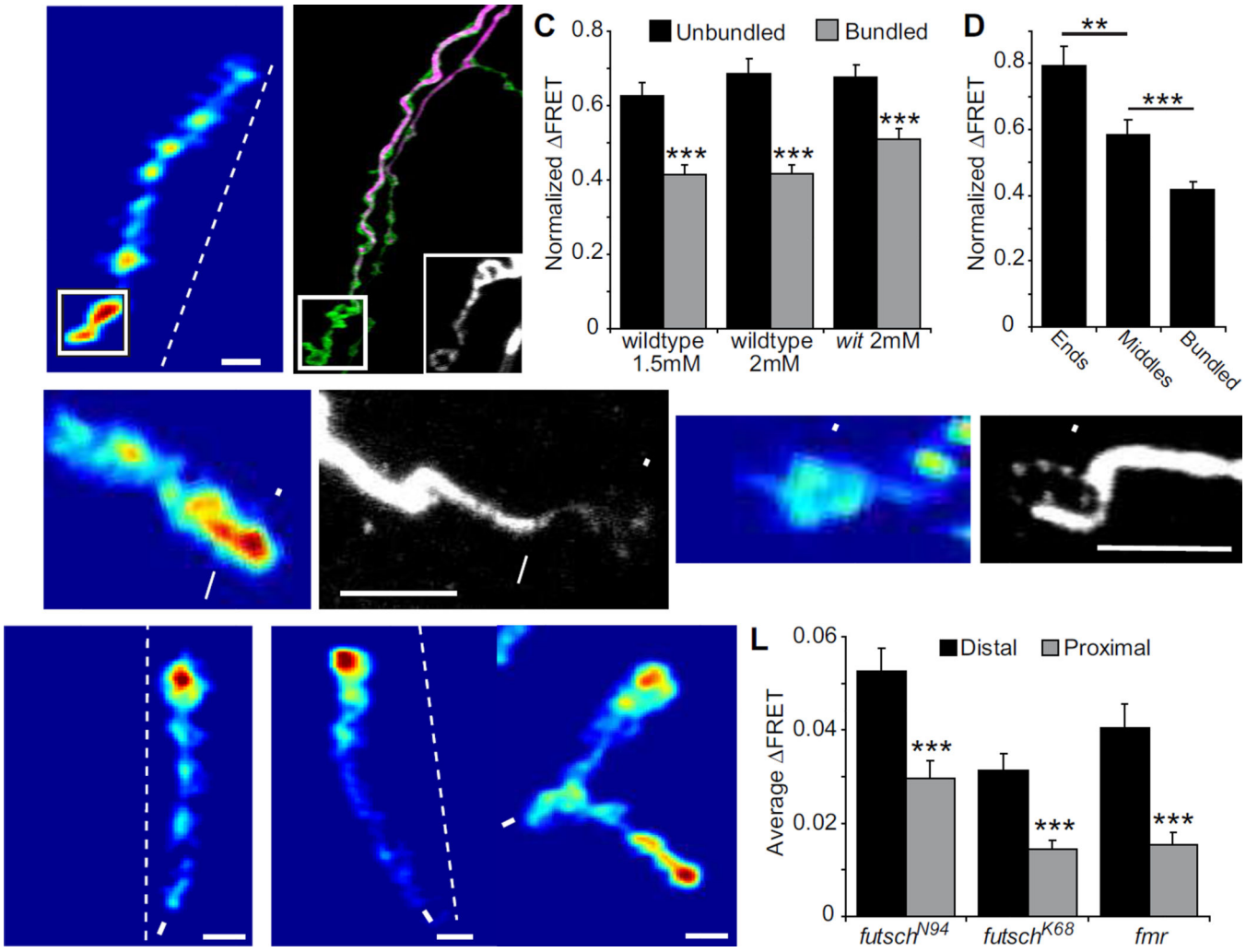

Figure 4.

Correlation between strong postsynapses and presynaptic loops of unbundled Futsch. (A–B) Example of a wildtype recording at 1.5 mM Ca^{2+}, where the boutons with the two strongest SynapCam responses also have loops of Futsch (scale:0–0.11). (B) Futsch is stained in purple, HRP in green and the inset is an enlarged image of the Futsch stain in the boxed region and at a higher gain. (C) Postsynapses in wildtype (at both 1.5 mM and 2 mM Ca^{2+}) and wit^{HA2}/wit^{HA3} mutants with unbundled presynaptic Futsch have a significantly larger average ΔFRET than those with bundled Futsch fibers (n > 40 postsynapses for every bar, p < 0.001 between unbundled and bundled for all genotypes). ΔFRET values were normalized to the strongest postsynapse in each NMJ. (D) End boutons and middle boutons with unbundled Futsch have larger ΔFRET than bundled Futsch. The data was taken from wildtype NMJs at 1.5 mM Ca^{2+}. (E–F) Example of strong bouton with bundled Futsch (arrow) next to strong bouton with faint diffuse Futsch staining (arrowhead). (G–H) Example of end bouton with loop of Futsch (arrowhead), but with low ΔFRET. The NMJs in (E–H) are from wildtype larvae recorded in 1.5 mM Ca^{2+} and scale bar = 5 μm. (I–K) Mean ΔFRET of (I) $futsch^{N94}$ hypomorph (scale: 0–0.045), (J) $futsch^{K68}$ null mutant (scale: 0–0.09) and (K) $fmr^{\Delta 113}/fmr^{\Delta 50}$ mutant (scale: 0.09), all recorded at 1.5 mM Ca^{2+} and −100

mV holding potential. (L) The synaptic gradient is not impaired in *futsch*^{N94} (n = 24), *futsch*^{K68} (n = 17) or *fmr*$^{\Delta 113}$/*fmr*$^{\Delta 50}$ (n = 26).

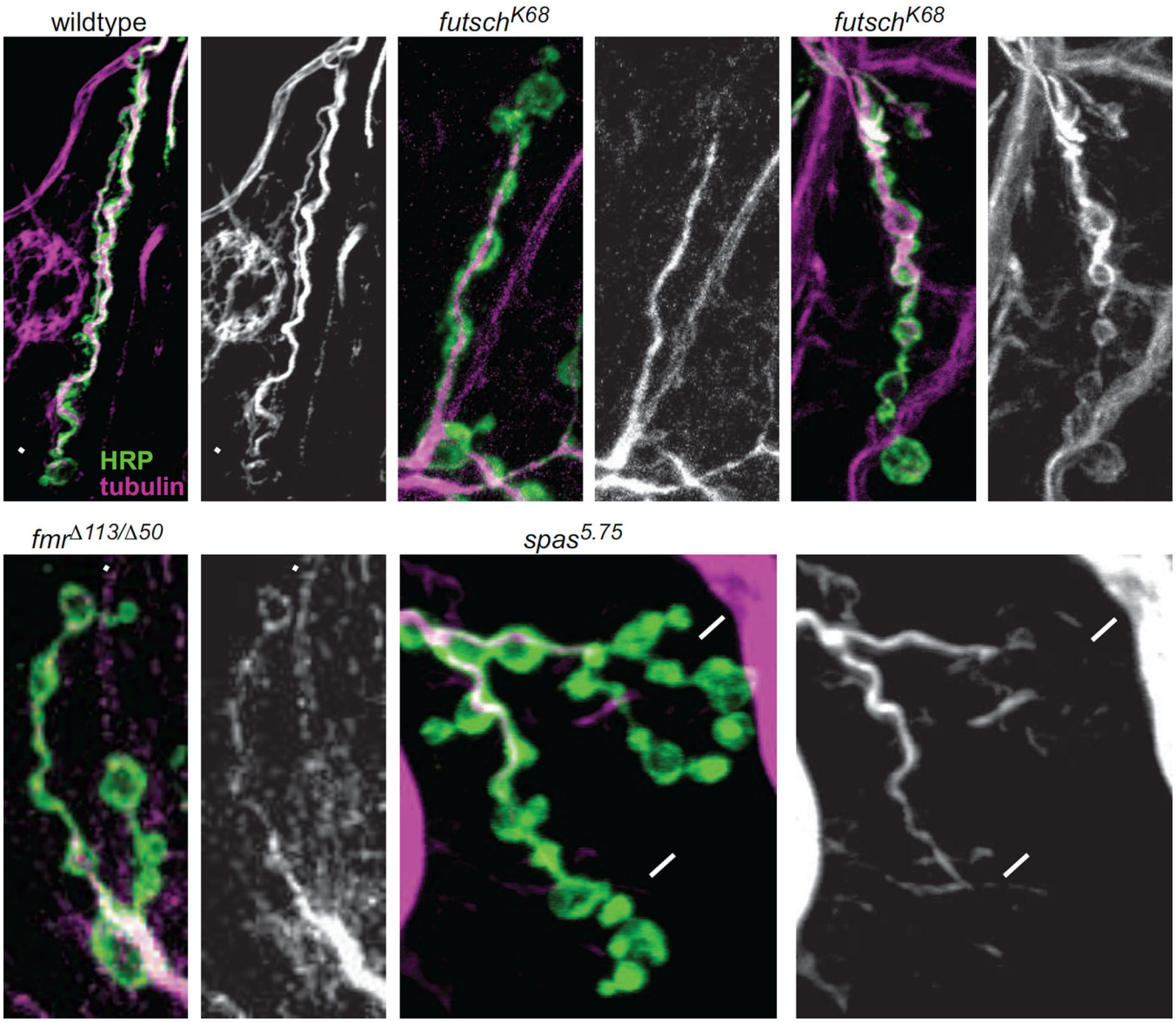

Figure 5.

Comparison of presynaptic microtubule organization in wildtype, *futsch*, *fmr* and *spastin*. HRP (green) and α-tubulin (purple or white) staining in (A) wildtype, (B–C) $futsch^{K68}$, (D) $fmr^{\Delta 113}/fmr^{\Delta 50}$ and (E) $spas^{5.75}$. Each genotype has an image of the double stain (1, left panels) and of tubulin alone (2, right panels). Arrowheads point to tubulin loops in the distal boutons. Arrows in E1–2 point to where the tubulin levels decrease below detection, towards the ends of the axons.

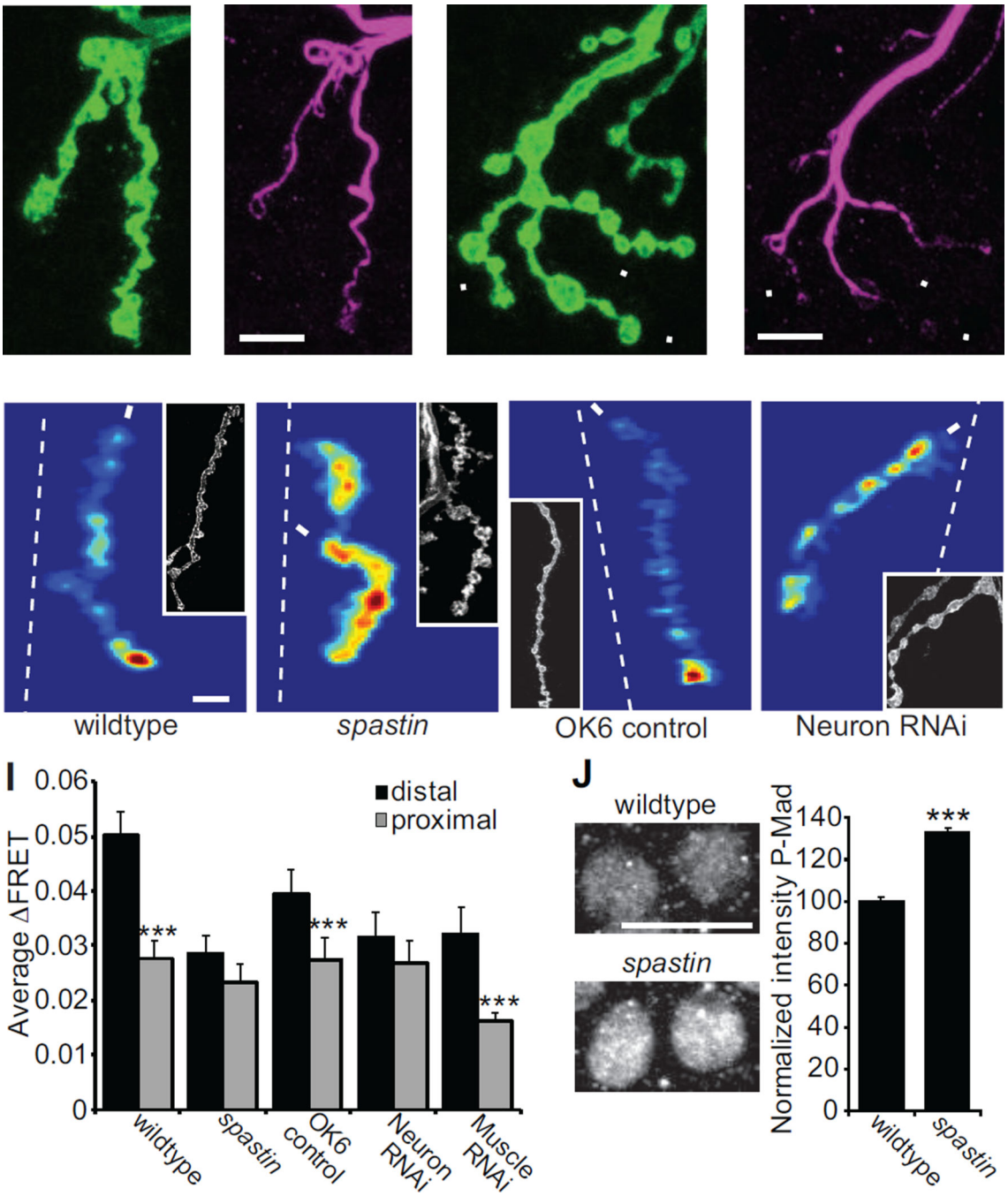

Figure 6.

spastin mutants lack the transmission gradient. (A,C) HRP (green) and (B,D) Futsch (purple) staining in (A–B) wildtype (C–D) and *spastin*$^{5.75}$. Microtubule organization is altered in *spastin* mutants. Often in *spastin* NMJs the levels of Futsch are barely detectable in distal boutons (arrowheads). (E–F) Mean ΔFRET of (E) wildtype (scale:0–0.09) and (F) *spastin* (scale:0–0.07) at 2 mM Ca^{2+} and −100 mV holding potential. (G–H) Mean ΔFRET of (G) OK6-Gal4/+ (scale: 0–0.055 for both panels) and (H) presynaptic Spastin RNAi (*SynapCam; OK6-Gal4/+; UAS-Spas-RNAi/+*) at 1.5 mM Ca^{2+} and −100 mV holding

potential. (I) Average ΔFRET for the distal and proximal postsynapses for the same genotypes as above, plus postsynaptic Spastin RNAi (*SynapCam;;24B-Gal4/UAS-Spas-RNAi*) ($n \geq 14$ for all). (J) P-Mad staining in motor neuron cell bodies is increased in $spastin^{5.75}$ mutants (n=9 larvae, 234 cells) compared to wildtype larvae (n=9 larvae, 234 cells). Images are of motor neuron cell bodies (the large round circles) in the ventral nerve cord stained with anti-P-Mad.

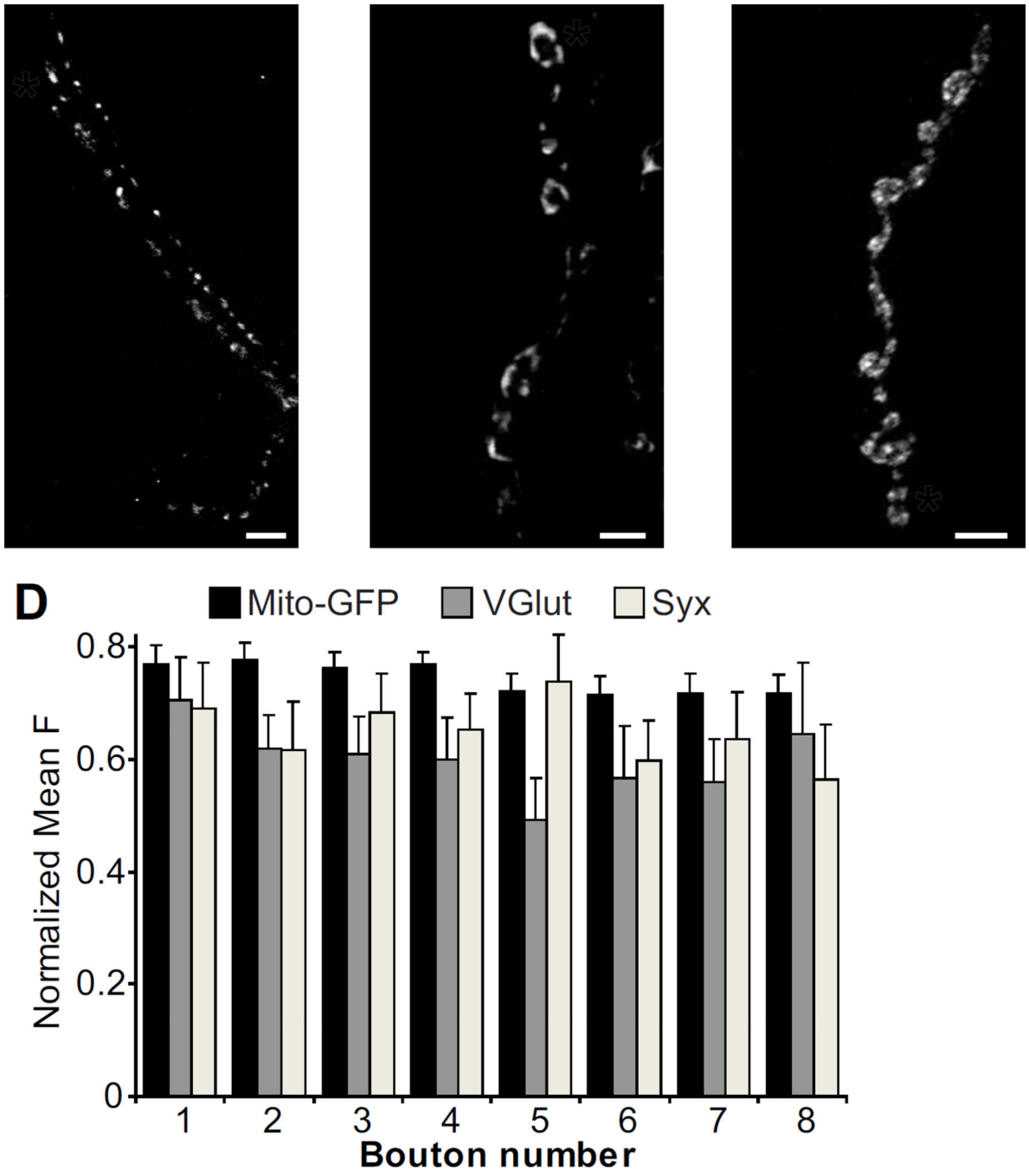

Figure 7.

There are no axonal gradients of mitochondria, synaptic vesicles, or a presynaptic T-SNARE. (A) NMJ expressing a GFP-tagged cytochrome C in motor neurons using D42-Gal4 to visualize mitochondria (*D42-Gal4, UAS-mito-GFP/TM6*). The asterisk indicates the distal bouton in a chain. (B–C) Wildtype NMJs stained for VGlut (B) and Syntaxin (C). (D) Quantification of mean fluorescence versus bouton position (Mito-GFP: n=35; VGlut: n=13; Syx: n=10).

Table 1

SynapCam recording conditions

Recording conditions for SynapCam imaging experiments.

Genotype	Figure	Extracellular Ca+2 (mM)	Holding Potential (mV)
Wildtype	1, 4A, 4E, 4G	1.5	−100
wit	1	1.5	−100
Wildtype	2A, 2D, 2F, 3A, 6E, 6I	2	−100
wit	2B, E, F	2	−120
Wit Rescue	2C, F	2	−100
Mad/+;wit/+	3D	1.5	−100
Mad	3B, C, D	2	−120
futsch	4I, J, L	1.5	−100
fmr	4K, L	1.5	−100
spastin	6F, I	2	−100
OK6 control	6G, I	1.5	−100
Spastin RNAi	6H, I	1.5	−100